

Numerical investigation of Mach number consistent Roe solvers for the Euler equations of gas dynamics

Friedemann Kemm

February 15, 2021

Keywords: Shock instability, Carbuncle phenomenon, Low Mach number effect, Low-dissipation schemes, Shock-capturing

MSC 2020: 76L05, 76M99, 76N15

While traditional approaches to prevent the carbuncle phenomenon in gas dynamics simulations increase the viscosity on entropy and shear waves near shocks, it was quite recently suggested to instead decrease the viscosity on the acoustic waves for low Mach numbers. The goal is to achieve what, in this paper, we call Mach number consistency: for all waves, the numerical viscosity decreases with the same order of the Mach number when the Mach number tends to zero. We take the simple approach that was used for the proof of concept together with the simple model for the increased numerical viscosity on linear waves and investigate the possibilities of combining both in an adaptive manner while locally maintaining Mach number consistency.

1 Introduction

Since the seminal paper of Quirk [41], an immense amount of research has been conducted on the instability problem that appears in the simulation of supersonic flow problems known as *Carbuncle Phenomenon*. The name originates from the fact that in strongly supersonic flows against an infinite cylinder simulated on a body-fitted, structured mesh the middle part of the resulting bow shock degenerates to a carbuncle-shaped structure. It was conjectured already by Quirk [41] that this phenomenon is closely related to other instabilities such as the so-called *odd-even-decoupling* encountered in straight shocks aligned

with the grid. The research in this area was twofold. On the one hand, the stability of discrete shock profiles was investigated in one as well as in several space dimensions [1, 3, 5, 6, 8, 10, 11, 15, 21, 22, 27, 29, 36, 38, 39, 42, 45, 49, 65]. On the other hand, there was a lot of effort spent to find cures for the failure of some schemes in numerical calculations [14, 20, 28, 30, 34, 35, 38–40, 46–48, 51, 52, 54, 56, 58, 60, 62–64]. Unfortunately, the failure is only found in schemes giving high resolution of shear and entropy waves by treating them explicitly, i. e. with so called *complete Riemann solvers* (as opposed to so called *incomplete Riemann solvers*), a category that includes, for example, the Godunov, Roe, Osher, HLLC and HLLEM schemes [9, 57]. Complete Riemann solvers are preferable in calculations involving complex wave structures as well as boundary layers.

It was found that even in one space dimension there are some instabilities of discrete shock profiles: slowly moving shocks produce small post-shock oscillations [1, 21, 41]. But also in the case of a steady shock, instabilities can be found depending on the value of the adiabatic coefficient γ as was shown by Bultelle et al. [5]. These and their relationship to two-dimensional instabilities of discrete shock profiles were our main focus in our earlier study on the sources of the carbuncle [27].

Another one-dimensional issue that was not yet considered in connection with the carbuncle, an issue that is also not studied in [27], is the wrong amplitude of pressure fluctuations normal to the flow direction that might arise from inconsistent numerical viscosities. This effect was brought to attention quite recently by Fleischmann et al. [13], who discuss the influence of what we will call *Mach number consistency*, namely requiring the viscosity on each wave to be of the same order $\mathcal{O}(M^\alpha)(M \rightarrow 0)$, on the stability of discrete shock profiles. While they force Mach number consistency in a strict manner, i. e. $\alpha = 2$, we loosen the definition of the term by only requiring the viscosity to be of the same order for all waves. In this sense, the traditional carbuncle cures are also Mach number consistent in the vicinity of discrete shock profiles by ensuring order $\mathcal{O}(M)$ for all viscosities.

In this study, we investigate the possibility of combining the two approaches $\mathcal{O}(M^2)$ and $\mathcal{O}(M)$ via an adaptive blending which would also allow $\mathcal{O}(M^{2-\beta})$ for some parameter $\beta \in [0, 1]$. As a starting point, we employ the simple modified Roe schemes proposed by Fleischmann et al. [13], which, although not leading to a production ready scheme, still allow for valuable insights into the problem and useful directions for further research. In Section 2, we discuss Mach consistent Roe solvers, wherein the basic properties of the Roe scheme are reviewed as well. Once a desired adaptive blending with numerical viscosity of order $\mathcal{O}(M^{2-\beta})$ and a computationally cheaper approximation by substituting the weighted geometric mean with a weighted arithmetic mean is achieved, we perform some numerical tests, cf. Section 3. These tests are chosen such that the desired information on the overall behaviour of the schemes can be extracted from their results. The ultimate goal as stated in Section 4 is to construct a robust all Mach number Roe solver that prevents the carbuncle, based on the insight gained in this study.

2 Mach number consistent Riemann solvers

2.1 The quasi linear form of the Euler equations

The Euler equations for an inviscid gas flow are

$$\begin{aligned}\rho_t + \nabla \cdot [\rho \mathbf{v}] &= 0, \\ (\rho \mathbf{v})_t + \nabla \cdot [\rho \mathbf{v} \circ \mathbf{v} + p \mathbf{I}] &= 0, \\ E_t + \nabla \cdot [(E + p) \mathbf{v}] &= 0\end{aligned}$$

with the density ρ , the velocity $\mathbf{v} = (u, v, w)^T$ for the 3d-case and $\mathbf{v} = (u, v)^T$ for the 2d-case, the pressure p , and the total energy E . Density, velocity, and pressure are called *primitive variables* in contrast to the *conserved variables* density, momentum, and total energy. Throughout this study, we consider the case of an ideal gas. The system is rotationally and Galilean invariant. Thus, it is sufficient so consider the quasi linear form

$$\mathbf{q}_x + \mathbf{A}^{(x)} \mathbf{q}_x + \mathbf{A}^{(y)} \mathbf{q}_y + \mathbf{A}^{(z)} \mathbf{q}_z, \quad (1)$$

where $\mathbf{A}^{(x)}, \mathbf{A}^{(y)}, \mathbf{A}^{(z)}$ are the flux Jacobians for the respective space directions, only for one space dimension, i. e. $\frac{\partial}{\partial y} = \frac{\partial}{\partial z} = 0$. Now, the eigenvalues of $\mathbf{A}^{(x)}$ are the wave speeds in x -direction, and the left and right eigenvectors determine the waves themselves.

Since we restrict our study to the two-dimensional case, we can drop the equation for the momentum in z -direction and end up with the wave speeds

$$\lambda_1 = u + c, \quad \lambda_2 = \lambda_3 = u, \quad \lambda_4 = u - c \quad (2)$$

with the speed of sound

$$c = \sqrt{\frac{\gamma p}{\rho}} = \sqrt{(\gamma - 1) \left(H - \frac{v^2}{2} \right)},$$

where γ is the ratio of specific heats and

$$H = \frac{E + p}{\rho} \quad (3)$$

the total enthalpy. The right eigenvectors of the flux Jacobian are

$$\mathbf{r}_1 = \begin{pmatrix} 1 \\ u - c \\ v \\ H - cu \end{pmatrix}, \quad \mathbf{r}_2 = \begin{pmatrix} 1 \\ u \\ v \\ \frac{1}{2} v^2 \end{pmatrix}, \quad \mathbf{r}_3 = \begin{pmatrix} 0 \\ 0 \\ 1 \\ v \end{pmatrix} \quad \mathbf{r}_4 = \begin{pmatrix} 1 \\ u + c \\ v \\ H + cu \end{pmatrix} \quad (4)$$

and the corresponding left eigenvectors

$$\begin{aligned}
l_1 &= \frac{1}{c(2H - v^2)} \left(Hu - \frac{(u-c)v^2}{2}, \frac{v^2}{2} - (H + cu), -cv, c \right), \\
l_2 &= \frac{1}{H - \frac{v^2}{2}} (H - v^2, u, v, -1), \\
l_3 &= (-v, 0, 1, 0), \\
l_4 &= \frac{1}{c(2H - v^2)} \left(-Hu + \frac{(u+c)v^2}{2}, -\frac{v^2}{2} + (H - cu), -cv, c \right).
\end{aligned} \tag{5}$$

In the following, we denote the matrix with the left eigenvectors as rows \mathbf{L} , the matrix with the right eigenvectors as columns \mathbf{R} , and keep in mind that we have normalized the eigenvectors such that $\mathbf{L} = \mathbf{R}^{-1}$.

2.2 Roe's consistent local linearization

If we write the generic 1d-scheme for a 1d conservation law

$$\mathbf{q}_t + \mathbf{f}(\mathbf{q})_x = \mathbf{0} \tag{6}$$

as

$$\frac{\mathbf{q}_i^{n+1} - \mathbf{q}_i^n}{\Delta t} + \frac{\mathbf{G}_{i+1/2}^n - \mathbf{G}_{i-1/2}^n}{\Delta x} = \mathbf{0}, \tag{7}$$

with the generic numerical flux function

$$\mathbf{G}(\mathbf{q}_r, \mathbf{q}_l) = \frac{1}{2}(\mathbf{f}(\mathbf{q}_r) + \mathbf{f}(\mathbf{q}_l)) - \frac{1}{2}\mathbf{V}(\mathbf{q}_r, \mathbf{q}_l)(\mathbf{q}_r - \mathbf{q}_l), \tag{8}$$

it is obvious that the matrix \mathbf{V} determines the numerical viscosity. If we now apply this to a linear system

$$\mathbf{q}_t + \mathbf{A}\mathbf{q}_x = \mathbf{0} \tag{9}$$

with constant system matrix \mathbf{A} and employ standard upwind on all waves, we end up with the viscosity matrix

$$\mathbf{V} = |\mathbf{A}|, \tag{10}$$

with the convention

$$|\mathbf{A}| = \mathbf{R}|\mathbf{A}|\mathbf{L}, \quad |\mathbf{A}| = \mathbf{diag}(|\lambda_1|, \dots, |\lambda_m|). \tag{11}$$

Thus, the absolute values of eigenvalues determine the numerical viscosity. This was the motivation for Roe [50] to look out for consistent local linearizations, i. e. a matrix $\tilde{\mathbf{A}} = \tilde{\mathbf{A}}(\mathbf{q}_l, \mathbf{q}_r)$ with the following properties

$$\mathbf{f}(\mathbf{q}_r) - \mathbf{f}(\mathbf{q}_l) = \tilde{\mathbf{A}}(\mathbf{q}_l, \mathbf{q}_r)(\mathbf{q}_r - \mathbf{q}_l), \tag{12}$$

$$\tilde{\mathbf{A}}(\mathbf{q}_l, \mathbf{q}_r) \rightarrow \mathbf{A}(\mathbf{q}) \quad \text{for } (\mathbf{q}_l, \mathbf{q}_r) \rightarrow (\mathbf{q}, \mathbf{q}), \tag{13}$$

$$\tilde{\mathbf{A}}(\mathbf{q}_l, \mathbf{q}_r) \text{ is diagonalizable for all } \mathbf{q}_l, \mathbf{q}_r. \tag{14}$$

A matrix $\tilde{A}(\mathbf{q}_l, \mathbf{q}_r)$ that satisfies these conditions is called a *Roe matrix* or a *consistent local linearization* for (6). If there exists a single state $\tilde{\mathbf{q}} = \tilde{\mathbf{q}}(\mathbf{q}_l, \mathbf{q}_r)$ with

$$\tilde{A}(\mathbf{q}_l, \mathbf{q}_r) = A(\tilde{\mathbf{q}}), \quad (15)$$

then it is called a *Roe mean value* for $\mathbf{q}_l, \mathbf{q}_r$. For the Euler equations, Roe found the following consistent mean values:

$$\begin{aligned} \tilde{\rho} &= \sqrt{\rho_l \rho_r}, \\ \tilde{u} &= \frac{\sqrt{\rho_l} u_l + \sqrt{\rho_r} u_r}{\sqrt{\rho_l} + \sqrt{\rho_r}}, \\ \tilde{v} &= \frac{\sqrt{\rho_l} v_l + \sqrt{\rho_r} v_r}{\sqrt{\rho_l} + \sqrt{\rho_r}}, \\ \tilde{w} &= \frac{\sqrt{\rho_l} w_l + \sqrt{\rho_r} w_r}{\sqrt{\rho_l} + \sqrt{\rho_r}}, \\ \tilde{H} &= \frac{\sqrt{\rho_l} H_l + \sqrt{\rho_r} H_r}{\sqrt{\rho_l} + \sqrt{\rho_r}}, \\ \tilde{c} &= \sqrt{(\gamma - 1) \left(\tilde{H} - \frac{1}{2} \tilde{v}^2 \right)} \end{aligned} \quad (16)$$

with $\tilde{v}^2 = \tilde{u}^2 + \tilde{v}^2 + \tilde{w}^2$ in the full three-dimensional case. For 2d, we simply omit the values for the third velocity component w .

A consequence of this is that the wave speeds in the Roe mean value determine the numerical viscosity. Since in the sonic point this turned out to be disadvantageous as upwinding in opposite direction leads to a sonic glitch, Harten [19] came up with the following fix: He replaces the absolute value of an eigenvalue λ of the Roe matrix by

$$\phi(\lambda) = \begin{cases} |\lambda| & \text{if } |\lambda| \geq \delta, \\ (\lambda^2 + \delta^2)/(2\delta) & \text{if } |\lambda| < \delta, \end{cases} \quad (17)$$

where δ is a small parameter. The numerical viscosity coefficient is here bounded below by $\delta/2$. Furthermore, we apply the fix only to the acoustic waves. In the test cases performed below, we found no visible difference in the numerical solutions.

2.3 Achieving Mach number consistency

Guillard and Viozat [18] show that for very small Mach numbers the viscosity resulting from the wave-wise upwind as in the standard Roe scheme leads to an inconsistency: While in the low Mach number limit pressure fluctuations scale with $\mathcal{O}(M^2)$, the numerical scheme supports pressure fluctuations of order $\mathcal{O}(M)$, where M is the reference Mach number of the flow field. Guillard and Viozat [18] identify the numerical viscosity as the source of this inconsistency, whereas Guillard and Murrone [17] use this as the starting point for a

preconditioner that modifies the numerical viscosities on the different waves such that they are of the same order. The crucial point is to reduce the viscosity on the acoustic waves to the same order as on the advective waves, the shear and entropy waves.

Fleischmann et al. [13] recommence this idea and suggest a simple low-dissipation modification for the acoustic waves to achieve what in the following we call *Mach number consistency*: In the low Mach number limit, the viscosities on all waves are of the same order. Note that this is a generalization of the original concept since we allow also for higher viscosities as long as they are of the same order for all waves. Keeping this terminology, Fleischmann et al. provide two basic strategies to maintain Mach number consistency in the Roe solver: a Mach number dependent upper bound for the viscosity on the nonlinear, i. e. acoustic, waves or a lower bound for the viscosity on the linear waves, i. e. entropy and shear waves. With a fixed positive number ϕ , the first approach, which is the main point of [13], leads to wave speeds

$$\tilde{\lambda}_{1,4} = \tilde{u} \mp \min\{\phi|\tilde{u}|, \tilde{c}\}, \quad \tilde{\lambda}_{2,3} = \tilde{u}, \quad (18)$$

the second to

$$\tilde{\lambda}_{1,4} = \tilde{u} \mp \tilde{c}, \quad \tilde{\lambda}_{2,3} = \text{sgn}(\tilde{u}) \max\left\{\frac{\tilde{c}}{\phi}, |\tilde{u}|\right\}. \quad (19)$$

It is easy to see that the approach resembles is a simplified model for the incomplete Riemann solvers traditionally used as a means to prevent the carbuncle. Only, for these the number ϕ is not fixed but depends on some type of indicator. While in the first case, for low Mach number flows, all eigenvalues of the viscosity matrix are $\mathcal{O}(u)$, in the latter case they are of the order $\mathcal{O}(c)$. The original purpose of Fleischmann et al. is to suggest the first approach as an alternative to the second. Their idea is that its application would in some sense reduce the transverse pressure fluctuations also in the vicinity of a shock and, thus, help to prevent the carbuncle phenomenon. In [12], they suggest a modified HLLC-scheme based on this approach.

One should at this point keep in mind that the second approach when naively applied also may lead to unphysical solutions [43], for purely low Mach number flows, the numerical viscosity might even outweigh the physical viscosity in a Navier-Stokes computation. So, it has to be handled with care.

On the other hand, the low dissipation approach might impair the numerical stability of the resulting scheme. It is well known (and can be found in standard text books, e. g. [31, 32, 57]) that in connection with the explicit Euler method as time Integration, the viscosities obtained from the wave-wise application of standard upwind are the lowest that would guarantee numerical stability. The situation might improve if some higher order time integration, e. g. some Runge Kutta method, is employed.

The question now arises if the two approaches might be combined in some way, i. e. imposing an upper bound to the acoustic speed and a lower bound to the absolute value of the flow speed at the same time while still maintaining Mach number consistency. For this

purpose, we suggest the following setting:

$$\tilde{\lambda}_{1,4} = \tilde{u} \mp \tilde{c}^\beta (\min \{ \phi |\tilde{u}|, \tilde{c} \})^{1-\beta}, \quad \tilde{\lambda}_{2,3} = \left(\text{sgn}(\tilde{u}) \max \left\{ \frac{\tilde{c}}{\phi}, |\tilde{u}| \right\} \right)^\beta \tilde{u}^{1-\beta}, \quad (20)$$

which is kind of a weighted geometric mean between the less and the more viscous approach that we call Mach number consistency. As desired, the order of the numerical viscosities for Mach numbers tending to zero is $\mathcal{O}(M^{2-\beta})$.

Since the low dissipation approach by Fleischmann et al. aims at the pressure perturbations perpendicular to the flow direction, while the traditional approach solely focuses on the possibility of a shock within the considered Riemann problem, it would be desirable to adapt the weights β and $1-\beta$ in a way that leads to the low dissipation approach in weakly compressible Riemann problems and the high dissipation approach in the presence of strong acoustic waves. For this purpose, like in our earlier work on the carbuncle [2, 23–25, 27], we resort to the residual in the Rankine-Hugoniot condition relative to the acoustic speed, i. e. in this case its Roe mean value. We find for the residual

$$\mathfrak{r} = \mathbf{f}(\mathbf{q}_r) - \mathbf{f}(\mathbf{q}_l) - \tilde{u}(\mathbf{q}_r - \mathbf{q}_l) \quad (21)$$

and from that

$$\frac{\mathfrak{r}}{\tilde{c}} = \lambda_4 \mathbf{r}_4 - \lambda_1 \mathbf{r}_1, \quad (22)$$

which is the difference between the right and left running acoustic waves. Instead of the more elaborate functions, which we have applied in our earlier work, we just compute β by

$$\beta = \min \left\{ \log_{10} \left(\max \left\{ \frac{\mathfrak{r}}{\tilde{c}}, 1 \right\} \right), 1 \right\}, \quad (23)$$

which is easily coded in any programming language since the common logarithm \log_{10} is usually available as an intrinsic function in the compilers as well as the natural logarithm. Since the residual vanishes for shear and entropy waves and is rather large for strong shocks, this choice of the weight β ensures that in the low Mach number regime we are left with the low dissipation approach, while a shock in the Riemann problem enforces the high dissipation Mach number consistent scheme.

Since the powers $(\cdot)^\beta$ and $(\cdot)^{1-\beta}$ in equation (8) are computationally expensive on most machines, in our numerical investigation, we also include an approximation of the weighted geometric mean: the corresponding weighted arithmetic mean

$$\tilde{\lambda}_{1,4} = \tilde{u} \mp \beta \tilde{c} + (1-\beta) \min \{ \phi |\tilde{u}|, \tilde{c} \}, \quad \tilde{\lambda}_{2,3} = \beta \text{sgn}(\tilde{u}) \max \left\{ \frac{\tilde{c}}{\phi}, |\tilde{u}| \right\} + (1-\beta)\tilde{u}. \quad (24)$$

Although this would not guarantee full Mach number consistency, it might still be a reasonable replacement at lower numerical cost.

3 Numerical investigation

In order to assess the behaviour of the simple prototypical Mach consistent Roe solvers discussed above, we perform a series of numerical tests. The test cases are chosen such that we can shed light on both the resolution of the resulting scheme and the stability of discrete shock profiles. Furthermore, we hope to find information on the possible loss in terms of numerical stability that might result from lowering the viscosity on the acoustic waves.

3.1 Overview of the test cases

Some of the tests can be performed in one space dimension while others are genuinely two-dimensional. For the sake of simplicity, we restrict ourselves to two dimensions and, thus, do not perform three-dimensional tests.

3.1.1 Steady shear wave

In order to investigate the resolution of the schemes, it is useful to consider a simple steady shear wave. A complete Riemann solver is expected to resolve steady shear waves exactly. In our tests, we modify the initial data by adding randomized numerical noise. While for the solver with the viscosity on shear and entropy waves bounded below, we expect the wave to be smeared out to some extent and for the solver with the viscosity on acoustic waves bounded to be exactly resolved, the main question is how the presence of the perturbations will affect the behaviour of the blended schemes. Is it sufficient to employ an indicator function in order to obtain results of the same quality as with the pure low viscosity scheme? The unperturbed initial data would be $\rho = 1$, $p = 1$, $u = 0$, $v_{r/l} = \pm 1$. The amplitude of the artificial noise is 10^{-6} . We will perform the test in two versions: purely one-dimensional and on the other hand two-dimensional where the shear wave is located on a grid line. This way, the 2d-version can be considered as a set of—except for the perturbations—identical 1d problems which somehow interact. This consideration will also be adopted when plotting the results of above tests.

3.1.2 Colliding flow

This test [33, Section 7.7] resembles a simplified model for the starting process of the blunt body test when using the inflow state as initial data in the complete computational domain. This is best understood when considering the flow before the blunt body along the symmetry line. Since the flow is aligned with that symmetry line, and due to the switch of the sign of the flow velocity for wall boundary conditions, it behaves essentially like the left half of a colliding flow in 1d. To turn it into a 2d-test, the flow is, again, equipped with an additional space direction, in which everything is expected to be constant. In

order to trigger the carbuncle, the initial state is superimposed with noise that is generated randomly and has a small amplitude.

For our numerical test, in the initial state, density and pressure are set to $\rho = 1$, $p = 1$. The normal velocity is set to $u_{\text{left/right}} = \pm 20$, the transverse velocity component to $v = 0$. To trigger the carbuncle, we superimpose artificial numerical noise of amplitude 10^{-6} onto the primitive variables instead of disturbing it in just one point as was done originally by LeVeque [33, Section 7.7]. The 2d computations are done on the rectangle $[0, 60] \times [0, 30]$ discretized with 60×30 grid cells. For the 1d computations, we just drop the second space dimension.

Since in 2d, the problem is a simple 2d-extension of the one-dimensional problem, the results are presented in scatter-type plots: we slice the grid in x -direction along the cell faces and plot the density for all slices at once.

3.1.3 Uniform flow

In its nature, this problem is similar to the two examples above: it is a 1d problem, which we artificially extend to two space dimensions. The basic flow is a uniform flow in x -direction but superimposed with artificial random numerical noise. We consider two examples, one with Mach number $M = 20$ and one with Mach number $M = 1/20$. Thus, we test the behaviour for highly supersonic as well as for weakly compressible flows. The unperturbed initial values for density and flow velocity (in x -direction) are $\rho = 1$, $u = 1$. The pressure is adjusted to the desired Mach number. The amplitude of the artificial noise is 10^{-6} .

3.1.4 Steady shock

While the colliding flow test models the starting process of the blunt body flow, the steady shock test, introduced by Dumbser et al. [8], features a simplified model for the converged shock in the blunt body flow. Following Dumbser et al., we set in the upstream region $\rho = 1$, $u = 1$. The upstream Mach number is set to $M = 20$, the transverse velocity component to $v = 0$, which again results in the 2d extension of a 1d problem. The shock is located directly on a cell face. To trigger the instability of the discrete shock profile, we add artificial numerical noise of amplitude 10^{-6} to the primitive variables in the initial state. The computations are done on $[0, 100] \times [0, 40]$ discretized with 100×40 grid cells.

Again for the presentation of the results, we also employ scatter-type plots as described for the colliding flow problem 3.1.2.

3.1.5 Quirk test

Quirk [41] introduced a test problem which is known as Quirk test. Contrary to the steady shear, the colliding flow, and the steady shock, it is not a one-dimensional Riemann problem, but consists of a shock running down a duct. The shock is caused by Dirichlet-type boundary conditions on the left boundary with $\rho = 5.26829268$, $u = 4.86111111$, $p = 29.88095238$,

while the flow field is initialized with $\rho = 1$, $u = v = 0$, $p = 1/\gamma$. Originally, a disturbance of the middle grid line was used to trigger the instability [41]. Because the computations are done with a Cartesian code, we instead use numerical noise in the same manner as for the steady shock and the colliding flow problem. The only difference lies in the amplitude of the perturbation, here 10^{-3} . The computations are done on $[0, 1600] \times [0, 20]$ discretized with 1600×20 grid cells. Again we use scatter-type plots (as described above) to present the results.

3.1.6 Elling test

Elling [11] investigates the influence of the supersonic upstream region on the shock profile. He models the interaction of a vortex filament with a strong shock. For this purpose, he starts with a steady shock. In the region upstream of the shock, he picks the middle slice of the computational grid and artificially sets the velocity to zero. For more details, we refer to our previous work [27]. The initial condition is a modified version of the steady shock test, cf. Section 3.1.4. The region to the right of the shock remains unchanged. In the supersonic inflow region, only the middle x -slice is changed. Here, the velocity is set to zero. This is done to model a vortex layer hitting the shock front, which in turn is a prototype for shock-boundary-layer interaction.

3.1.7 Kelvin-Helmholtz instability

For the Kelvin-Helmholtz instability, we start with a flow which consists of three parts. In a region close to the middle line, it is uniformly directed towards the left with $u = -\sqrt{\gamma}/2$. Above and below, it is directed in the opposite direction with $u = \sqrt{\gamma}/2$. Pressure and density are constant everywhere with $p = 1$ and $\rho = 1$. To trigger the instability, we slightly disturb the y -component of the flow velocity. The perturbation is sinusoidal in x -direction with an amplitude of $1/100$ and constant in y -direction. However, as we cannot expect for a first order scheme that the instability will evolve on our given 100×100 grid, we resort to a second order scheme with direction-wise minmod on primitive variables. Since this example is dominated by entropy and shear waves, it is a good test for the overall resolution of the scheme. Furthermore, it features a low Mach number flow, which allows us to evaluate the robustness of the scheme and how much fragility might arise from the upper bound for the viscosity on the acoustic waves.

3.1.8 Double Mach Reflection (DMR)

The Double Mach Reflection is a self similar solution that evolves from a shock running up a ramp. It was introduced by Woodward and Colella [59] as a benchmark for Euler codes. In contrast to the single Mach reflection, the double Mach reflection features two triple points and, thus, is a challenging problem for gas dynamics codes. Here, only a brief overview is given since this problem has already been discussed in more detail in our earlier work [26].

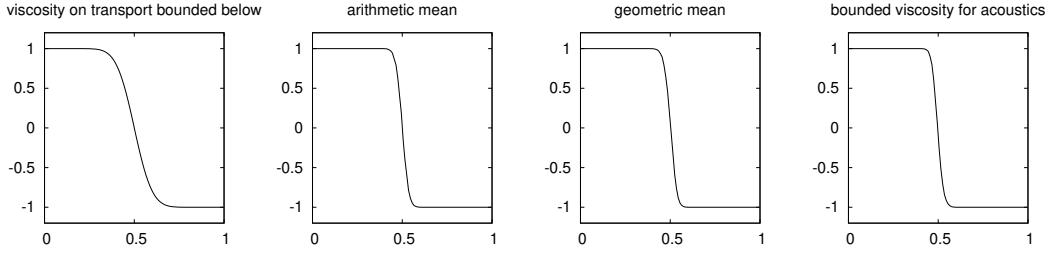


Figure 1: Transverse velocity for steady shear wave with randomized noise at time $t = 2.5$

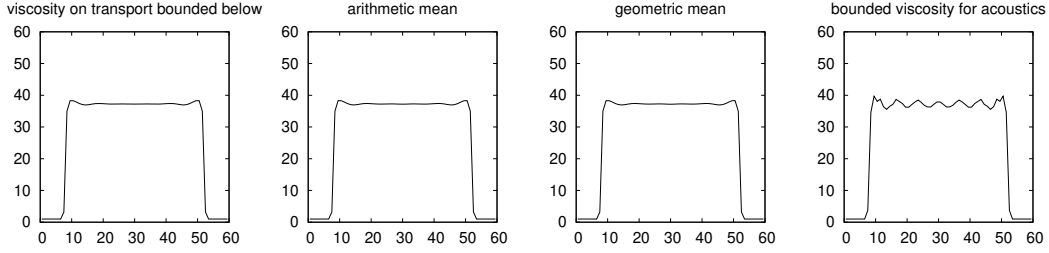


Figure 2: Colliding flow at time $t = 30$

As suggested therein, we double the size of the computational domain in the y -direction and also follow the other suggestions made in that study. The results are displayed as contour plots of the transverse momentum ρv , which gives the best insight into the quality of the scheme. This is especially true for the resolution of the secondary slip line.

3.2 Numerical results and discussion

For the numerical results, we employed Euler2d, a simple 2d-Cartesian code developed for the test of Riemann solvers in the Group of Claus-Dieter Munz at Stuttgart University. The code implements standard finite volumes. For higher order, direction-wise geometric limiting with minmod on primitive variables is used.

3.2.1 One-dimensional tests

In this section, we consider two tests: a perturbed steady shear wave and a colliding flow. While the purpose of the shear wave test is obvious, the purpose of the latter is to check for issues, that the lowered viscosity on the acoustic waves might cause. The results for the **perturbed steady shear wave** in Figure 1 clearly show that the indicator function β nicely detects the absence of shocks and, thus, avoids unnecessary viscosity on the shear wave. Except for the high viscosity approach, all versions show the same result.

In Figure 2, for the **colliding flow** test, we find the opposite situation: here, all versions except for the original Fleischmann solver yield the same results. If the viscosity on the

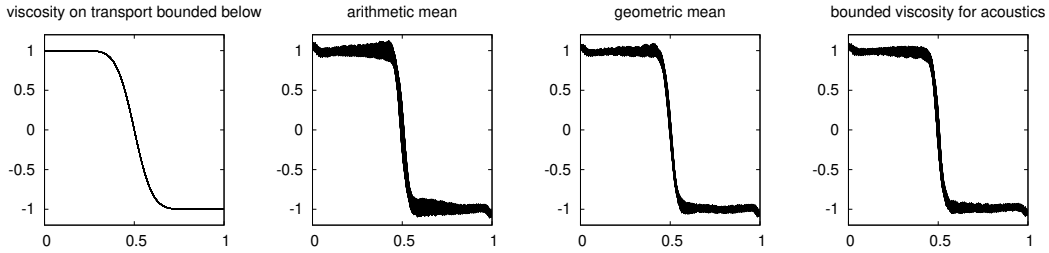


Figure 3: Steady shear wave with randomized noise at time $t = 2.5$

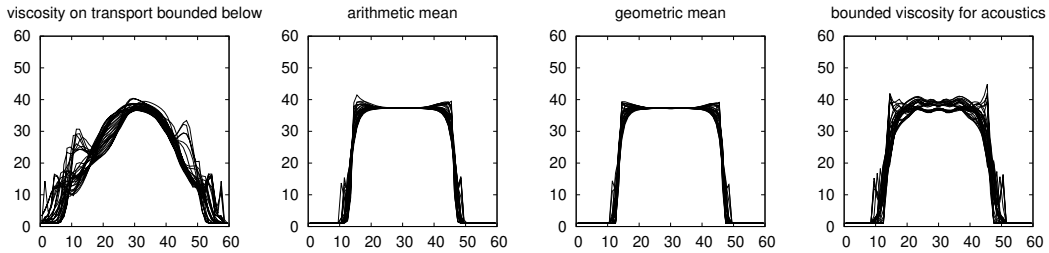


Figure 4: Colliding flow at time $t = 30$

acoustic waves is bounded regardless of the presence or absence of strong acoustic waves, we suffer from a strong increase of post-shock oscillations.

3.2.2 2d counterparts of 1d tests and other quasi one dimensional 2d tests

Since these tests are simple 2d-extensions of one-dimensional problems, the results are presented in scatter-type plots: we slice the grid in x -direction along the cell faces and plot the density or, in the case of the perturbed shear wave, the transverse velocity for all slices at once.

As can be seen in Figure 3, the 2d **perturbed steady shear wave** reveals that the strict application of a lower bound for the transport viscosity at the one hand leads to a strong smearing effect on the shear wave but on the other hand prevents perturbations in y -direction. Furthermore, we indeed observe a slight difference between the application of the arithmetic and the geometric mean. As we will see, this is typical for situations without strong acoustic waves.

For the 2d **colliding flow**, as depicted in Figure 4, we get quite reasonable, but not yet perfect, results with the blended schemes. An interesting point is that the low dissipation version yields better results than the high viscosity variant. This is surprising, especially with respect to the purely one-dimensional results in Section 3.2.1.

For the **uniform flow**, we present results for both the $M = 20$ and the $M = 1/20$ flow in Figures 5 and 6, respectively. While for the former the differences between the blended and the low dissipation schemes are rather small, for the latter they are significant. Also, the differences between the geometric and the arithmetic mean are clearly visible. Although

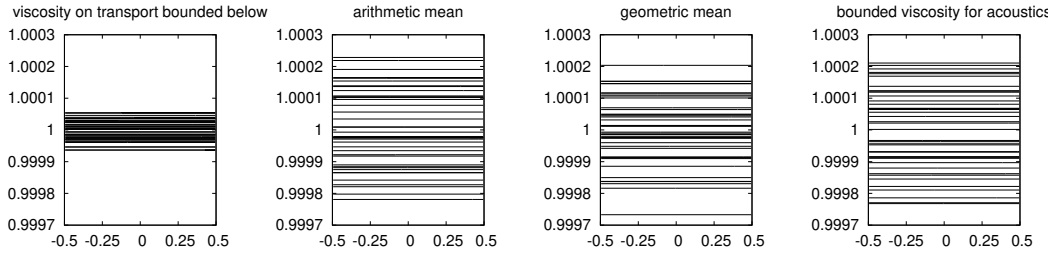


Figure 5: Supersonic uniform flow with randomized noise at time $t = 5$

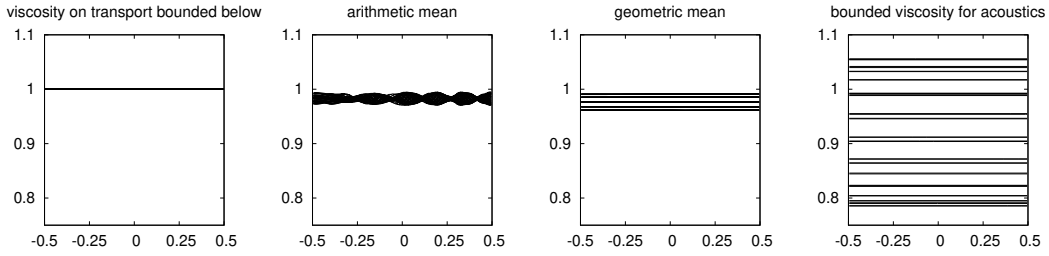


Figure 6: Subsonic uniform flow with randomized noise at time $t = 5$

the amplitude of the perturbations is about the same, the version with the geometric mean shows only variations in the transverse direction while the variant with the arithmetic mean features a more complex flow pattern.

The test case with the **steady shock** is well resolved by all solvers, cf. Figure 7. With the high viscosity method, which is intended to serve as a simplified model for the traditional carbuncle cures, the results are quite similar to those of the carbuncle cures which rely on an indicator computed from the Riemann problem itself, e. g. our own HLEMCC solver [23]. Even the blended and the low dissipation schemes yield perfect results. This confirms that there indeed is, as stated by Fleischmann et al. [13], a significant influence of the post shock region on the stability of the discrete shock profile. Furthermore, it seems even better to opt for the low dissipation Mach consistent numerical flux than for the traditional high dissipation approach.

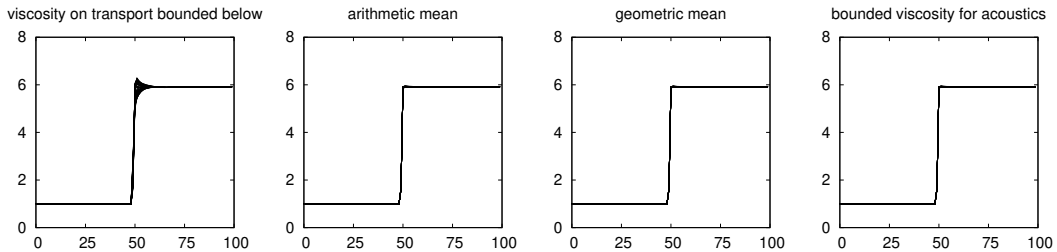


Figure 7: Steady shock test at time $t = 100$

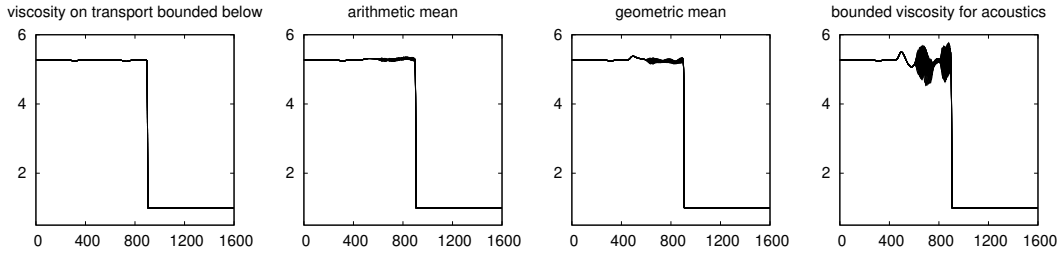


Figure 8: Quirk test at time $t = 150$

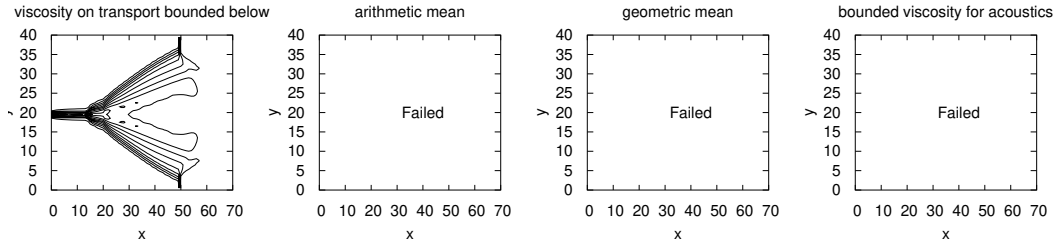


Figure 9: Density for Elling test at time $t = 100$; 1st order computation

As can be seen in Figure 8, the results for the **Quirk test** (cf. Section 3.1.5) show some similarity with the well known shock entropy wave interaction problem as suggested by Shu and Osher test [55], where a moving shock interacts with density fluctuations of small amplitude. While for the version with the transport viscosity bounded below the results look perfect, the effect is clearly visible for the strict low dissipation Roe solver. For the blended schemes, it is still visible but with a much smaller amplitude. This indicates that the lowered viscosity on the acoustics in the resting fluid right of the shock causes slight numerical instabilities which lead to an increase of the density perturbations introduced by the artificial noise in the initial state.

Furthermore, as for the low Mach number uniform flow in Figure 6, we observe a difference between the blended versions with geometric and arithmetic mean. This might be due to the fact that the perturbed resting fluid resembles the situation of the Mach number uniform flow closely. In fact, it is a flow field with extremely low Mach number.

3.2.3 Genuinely two-dimensional test cases

Here, we discuss some problems that are genuinely two-dimensional, which means that they have no one-dimensional counterpart. They allow us to study how the results we have gotten so far adapt to more real-life situations with complex flow structures. Since the problems are genuinely 2d, we also have to resort to genuinely 2d-types of plots. In most cases, we show contour plots, while for one example a surface plot is also provided since the contour plot alone would be somehow misleading.

In the **Elling test** (Figure 9), we can see the stability issues introduced by the low

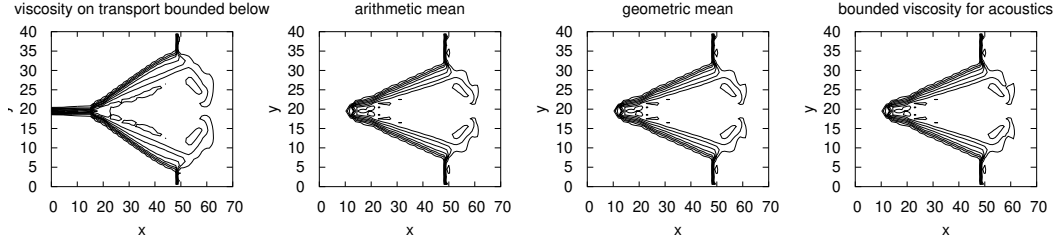


Figure 10: Entropy for Elling test at time $t = 100$; 2nd order computation

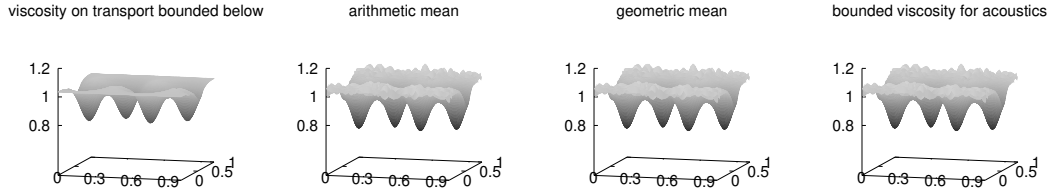


Figure 11: Entropy for Kelvin-Helmholtz instability at time $t = 4$, surface plot

dissipation on the acoustic waves. All first order computations except for the high dissipation method abort after some time, which is however fixed by the increase of the order of the scheme, as can be seen in Figure 10. This also might explain why in their studies Fleischmann et al. [12, 13] did not observe any stability issues: they employed fifth order in space and third order in time. For the SSP-Runge-Kutta, they use for the time integration, no details are given by Fleischmann et al. [13]. But there is a good chance that also the stability region is shaped in a way that provides additional stability. As a comparison to the results in [27] shows, while the result of the high dissipation closely resembles our old carbuncle cure, HLEMCC [23], the other versions resemble the results obtained with the Osher solver.

The results for the **Kelvin-Helmholtz** instability (cf. Section 3.1.7) show a better resolution of the instability itself when the transport viscosity is not bounded below in weakly compressible flows (Figure 11). But on the other hand, and much more prominent, at least when the contours are plotted as in Figure 12, some instabilities indicate that the naive approach for lowering the viscosity on acoustic waves as studied in this paper is not sufficient. Like for the low Mach uniform flow and the Quirk test as well as the Elling test, one would ask for a more elaborate way of adjusting the acoustic viscosity, maybe by adapting the parameter ϕ in some way.

Finally, we show results for the **double Mach reflection** as described in Section 3.1.8. While Figure 13 displays the results of the first order computation, Figure 14 provides the results obtained with second order in space and time. We performed computations with a grid spacing of $\Delta x = \Delta y = 1/120$, $\Delta x = \Delta y = 1/240$, and $\Delta x = \Delta y = 1/480$,

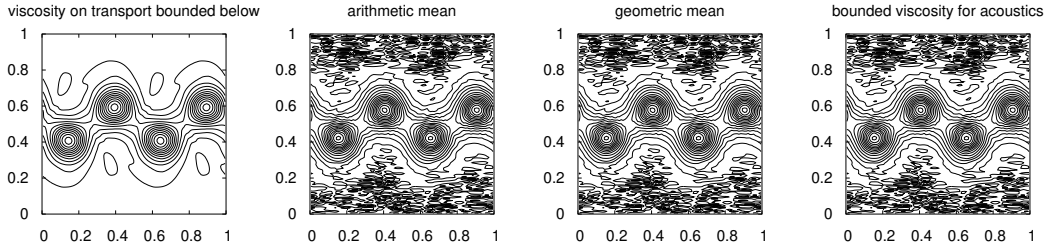


Figure 12: Density for Kelvin-Helmholtz instability at time $t = 4$, contour plot

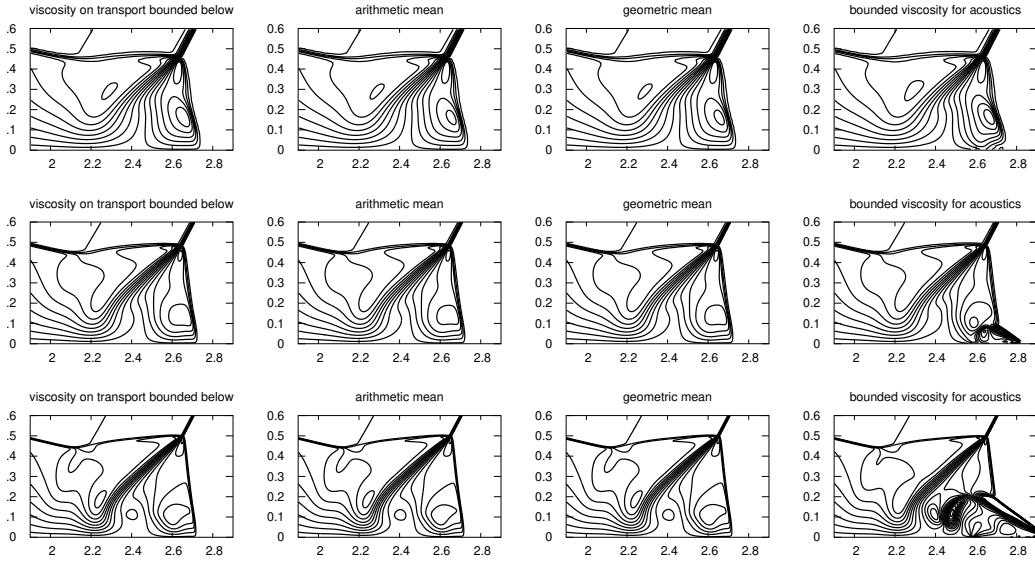


Figure 13: Vertical momentum for Double Mach Reflection problem; 1st order computations with $\Delta x = \Delta y = 1/120$, $\Delta x = \Delta y = 1/240$, and $\Delta x = \Delta y = 1/480$ (from top to bottom)

where the latter is the standard resolution for the DMR test as introduced by Woodward and Colella [59]. The most prominent feature in the results is the kinked Mach stem originating from a carbuncle in the computations with the pure low dissipation approach. This indicates that, in order to safely prevent a carbuncle, it is still necessary to increase the viscosity on shear and entropy waves in the vicinity of strong shocks. Fighting one possible source of the carbuncle seems not sufficient. In fact, it seems to be crucial to address all possible sources at the same time in order to get optimal results.

For the second order computations the situation is much better, as no carbuncle can be found. Furthermore, the differences between the schemes are much smaller, and the secondary slip line can be seen in all of them, especially with $\Delta x = \Delta y = 1/480$. According to our earlier findings in [27, § 5.2], the higher order already stabilizes the shock position. Although minmod is rather weak in this respect, for the DMR, it seems sufficient to provide

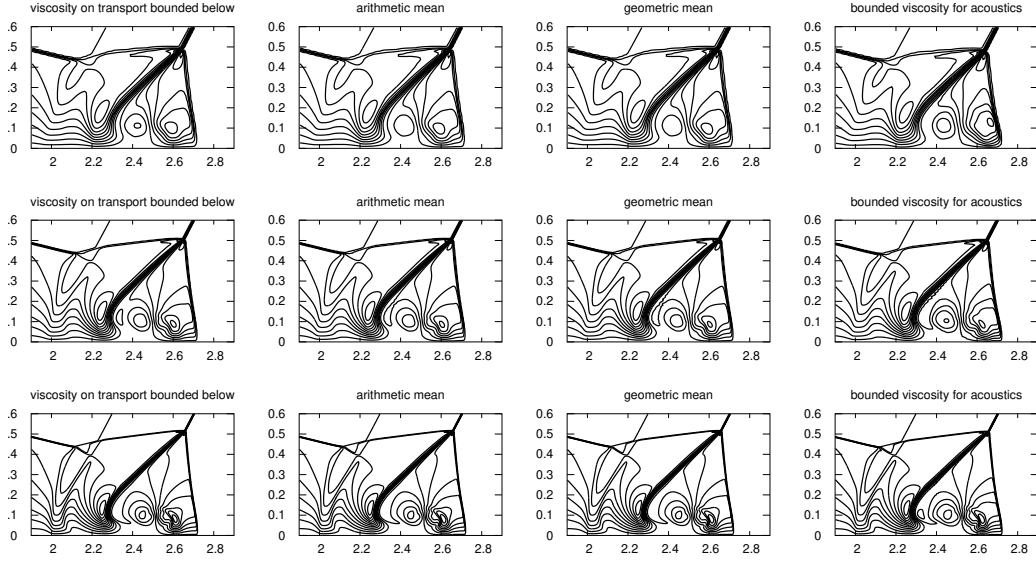


Figure 14: Vertical momentum for Double Mach Reflection problem; 2nd order computations with $\Delta x = \Delta y = 1/120$, $\Delta x = \Delta y = 1/240$, and $\Delta x = \Delta y = 1/480$ (from top to bottom)

the necessary additional stabilization.

4 Conclusions and possible directions for further research

We started with the work of Fleischmann et al. [13] and their simplified models for low Mach number corrections (18) and carbuncle preventing incomplete Riemann solvers (19) and combined them via the blending (20) or its computationally cheaper approximation (24) in connection with the indicator (23) to investigate the influence of Mach number consistency on the carbuncle phenomenon. The parameter β was introduced to provide a smooth transition between the low dissipation scheme for weakly compressible and the high dissipation method for fully compressible Riemann problems. It should be kept in mind that in high-speed grid aligned flows both cases occur at the same time, depending on the space direction.

The first results look rather promising. For many test cases, at least when the order of the scheme is increased, the schemes perform well. For the steady shock problem, the perturbations along the shock front were much smaller than with traditional carbuncle cures based solely on the use of a higher viscosity for shear and entropy waves near shocks. In some test cases like the Elling test, where all except the high dissipation scheme failed in the 1st order computations, as well as the Quirk test (mainly the pure low dissipation version) and the Kelvin-Helmholtz instability, perturbations caused by the violation of the

stability conditions as a result of lowering the viscosity below the Roe values can be seen. Addressing this issue seems to be the most important contribution expected from future research.

Since there is ongoing and vivid research towards Riemann solvers for low Mach number flows, e. g. [4, 7, 12, 16, 37, 44, 53, 61], there is also hope that in the near future a way will be found to construct a robust all Mach number Riemann solver that prevents unphysical carbuncles based on the above considerations. Although Xie et al. [61] do not explicitly control Mach number consistency, their solver can already be considered a step in this direction.

In some cases, the experimental solver used in this study might be sufficient: High order SSP/monotone time integration schemes, and many high order Runge-Kutta schemes in general, tend to provide some sort of reserve in terms of stability, something the explicit Euler scheme lacks for all modes of the semi-discrete system obtained by first order standard upwind. As the original results by Fleischmann et al. [13] and the results for their modified HLLC-solver [12] show, for most computations, this seems to be sufficient even when the low dissipation version (18) is applied in its pure form. Thus, we conclude that the blended schemes can also be safely used in many very high order gas dynamics codes.

References

- [1] Mohit Arora and Philip L. Roe, *On postshock oscillations due to shock capturing schemes in unsteady flows*, *Journal of Computational Physics* **130** (1997), 25–40.
- [2] Georg Bader and Friedemann Kemm, *The carbuncle phenomenon in shallow water simulations*, The 2nd International Conference on Computational Science and Engineering (ICCSE-2014) (Ho Chi Minh City, Vietnam), 2014.
- [3] Derek S. Bale and Christiane Helzel, *Crossflow instabilities in the approximation of detonation waves*, *Hyperbolic Problems: Theory, Numerics, Applications* (Basel - Boston - Berlin) (Heinrich Freistühler and Gerald Warnecke, eds.), International Series of Numerical Mathematics, vol. 141, Birkhäuser Verlag, 2001, pp. 119–128.
- [4] Wasilij Barsukow, Philipp V. F. Edelmann, Christian Klingenberg, Fabian Miczek, and Friedrich K. Röpke, *A numerical scheme for the compressible low-Mach number regime of ideal fluid dynamics*, *Journal of Scientific Computing* **72** (2017), no. 2, 623–646.
- [5] Matthieu Bultelle, Magali Grassin, and Denis Serre, *Unstable Godunov discrete profiles for steady waves*, *SIAM Journal on Numerical Analysis* **35** (1998), no. 6, 2272–2297.
- [6] Y. Chauvat, Jean-Marc Moschetta, and Jérémie Gressier, *Shock wave numerical structure and the carbuncle phenomenon*, *International Journal for Numerical Methods in Fluids* **47** (2005), 903–909.

- [7] S. Dellacherie, J. Jung, P. Omnes, and P.-A. Raviart, *Construction of modified Godunov-type schemes accurate at any Mach number for the compressible Euler system*, *Mathematical Models and Methods in Applied Sciences* **26** (2016), no. 13, 2525–2615.
- [8] Michael Dumbser, Jean-Marc Moschetta, and Jérémie Gressier, *A matrix stability analysis of the carbuncle phenomenon*, *Journal of Computational Physics* **197** (2004), 647–670.
- [9] Bernd Einfeldt, *On Godunov-type methods for gas dynamics.*, *SIAM J. Numer. Anal.* **25** (1988), no. 2, 294–318 (English).
- [10] Volker Elling, *Carbuncles as self-similar entropy solutions*, arXiv:math/0609666 (2006).
- [11] ———, *The carbuncle phenomenon is incurable*, *Acta Mathematica Scientia* **29** (2009), no. 6, 1647–1656.
- [12] Nico Fleischmann, Stefan Adami, and Nikolaus A. Adams, *A shock-stable modification of the HLLC Riemann solver with reduced numerical dissipation*, *Journal of Computational Physics* **423** (2020), 109762.
- [13] Nico Fleischmann, Stefan Adami, Xiangyu Y. Hu, and Nikolaus A. Adams, *A low dissipation method to cure the grid-aligned shock instability*, *Journal of Computational Physics* **401** (2020), 109004.
- [14] Jesús Garicano-Mena, Andrea Lani, and Herman Deconinck, *An energy-dissipative remedy against carbuncle: Application to hypersonic flows around blunt bodies*, *Computers & Fluids* **133** (2016), 43–54.
- [15] Jérémie Gressier and Jean-Marc Moschetta, *Robustness versus accuracy in shock-wave computations*, *International Journal for Numerical Methods in Fluids* **33** (2000), 313–332.
- [16] H. Guillard and B. Nkonga, *Chapter 8 – on the behaviour of upwind schemes in the low Mach number limit: A review*, *Handbook of Numerical Methods for Hyperbolic Problems* (Rémi Abgrall and Chi-Wang Shu, eds.), *Handbook of Numerical Analysis*, vol. 18, Elsevier, 2017, pp. 203–231.
- [17] Hervé Guillard and Angelo Murrone, *On the behavior of upwind schemes in the low Mach number limit: II. Godunov type schemes*, *Computers & fluids* **33** (2004), 655–675.
- [18] Hervé Guillard and Cécile Viozat, *On the behaviour of upwind schemes in the low Mach number limit*, *Computers & fluids* **28** (1999), no. 1, 63–86.
- [19] Ami Harten, *High resolution schemes for hyperbolic conservation laws.*, *J. Comput. Phys.* **49** (1983), 357–393 (English).

- [20] Kuibang Huang, Hao Wu, Heng Yu, and Dong Yan, *Cures for numerical shock instability in HLLC solver.*, *Int. J. Numer. Methods Fluids* **65** (2011), no. 9, 1026–1038.
- [21] Shi Jin and Jian-Guo Liu, *The effects of numerical viscosities i: Slowly moving shocks*, *Journal of Computational Physics* **126** (1996), 373–389.
- [22] Iraj M. Kalkhoran and Michael K. Smart, *Aspects of shock wave-induced vortex breakdown*, *Progress in Aerospace Sciences* **36** (2000), no. 1, 63–95.
- [23] Friedemann Kemm, *A carbuncle free Roe-type solver for the Euler equations.*, Benzoni-Gavage, Sylvie (ed.) et al., *Hyperbolic problems. Theory, numerics and applications. Proceedings of the 11th international conference on hyperbolic problems*, Ecole Normale Supérieure, Lyon, France, July 17–21, 2006. Berlin: Springer, 2008, pp. 601–608.
- [24] ———, *Contributions to the numerical simulation of gas, shallow water, and plasma flows – wave-wise treatment of order and viscosity*, Habilitationsschrift, Brandenburgische Technische Universität, 2014.
- [25] ———, *A note on the carbuncle phenomenon in shallow water simulations*, *ZAMM - Journal of Applied Mathematics and Mechanics / Zeitschrift für Angewandte Mathematik und Mechanik* **94** (2014), no. 6, 516–521.
- [26] ———, *On the proper setup of the double Mach reflection as a test case for the resolution of gas dynamics codes*, *Computers & Fluids* **132** (2016), 72–75.
- [27] ———, *Heuristical and numerical considerations for the carbuncle phenomenon*, *Appl. Math. Comput.* **320** (2018), no. Supplement C, 596–613.
- [28] Sung-Soo Kim, Chongam Kim, Oh-Hyun Rho, and Seung Kyu Hong, *Cures for the shock instability: Development of a shock-stable roe scheme*, *Journal of Computational Physics* **185** (2003), 342–374.
- [29] Keiichi Kitamura, *A further survey of shock capturing methods on hypersonic heating issues*, *AIAA Paper* **2698** (2013).
- [30] Keiichi Kitamura, Philip Roe, and Farzad Ismail, *Evaluation of Euler fluxes for hypersonic flow computations*, *AIAA Journal* **47** (2009), no. 1, 44–53.
- [31] Culbert B. Laney, *Computational gasdynamics.*, Cambridge: Cambridge University Press, 1998.
- [32] Randall J. LeVeque, *Finite volume methods for hyperbolic problems.*, Cambridge Texts in Applied Mathematics. Cambridge: Cambridge University Press, 2002 (English).
- [33] Randall J. LeVeque, Dimitri Mihalas, E. A. Dorfi, and Ewald Müller, *Computational methods for astrophysical fluid flow*, Springer, Berlin, Heidelberg, 1998.

- [34] Ching Y. Loh and Philip CE Jorgenson, *A time-accurate upwind unstructured finite volume method for compressible flow with cure of pathological behaviors*, AIAA paper **4463** (2007).
- [35] J.C. Mandal and V. Panwar, *Robust HLL-type Riemann solver capable of resolving contact discontinuity*, *Computers & Fluids* **63** (2012), 148–164.
- [36] J.-M. Moschetta, J. Gressier, J.-C. Robinet, and G. Casalis, *The carbuncle phenomenon: a genuine Euler instability?*, Toro, E. F. (ed.), *Godunov methods. Theory and applications. International conference, Oxford, GB, October 1999*. New York, NY: Kluwer Academic/Plenum Publishers. 639-645 (2001)., 2001.
- [37] K. Oßwald, A. Siegmund, P. Birken, V. Hannemann, and A. Meister, *L^2 Roe: a low dissipation version of Roe’s approximate Riemann solver for low Mach numbers*, *International Journal for Numerical Methods in Fluids* **81** (2016), no. 2, 71–86.
- [38] Maurizio Pandolfi and Domenic D’ Ambrosio, *Numerical instabilities in upwind methods: Analysis and cures for the carbuncle phenomenon*, *Journal of Computational Physics* **166** (2001), no. 2, 271–301.
- [39] Soo Hyung Park and Jang Hyuk Kwon, *On the dissipation mechanism of Godunov type schemes*, *Journal of Computational Physics* **188** (2003), 524–542.
- [40] Sutthisak Phongthanapanich and Pramote Dechaumphai, *Healing of shock instability for Roe’s flux-difference splitting scheme on triangular meshes.*, *Int. J. Numer. Methods Fluids* **59** (2009), no. 5, 559–575.
- [41] James J. Quirk, *A contribution to the great Riemann solver debate*, *International Journal for Numerical Methods in Fluids* **18** (1994), 555–574.
- [42] Marcus Ramalho and Joao Luiz Azevedo, *A possible mechanism for the appearance of the carbuncle phenomenon in aerodynamic simulations*, 48th AIAA Aerospace Sciences Meeting Including the New Horizons Forum and Aerospace Exposition, 2010.
- [43] Felix Rieper, *On the dissipation mechanism of upwind-schemes in the low Mach number regime: A comparison between Roe and HLL*, *Journal of Computational Physics* **229** (2010), no. 2, 221–232.
- [44] ———, *A low-Mach number fix for Roe’s approximate Riemann solver*, *Journal of Computational Physics* **230** (2011), no. 13, 5263–5287.
- [45] Jean-Christophe Robinet, Jérémie Gressier, G. Casalis, and Jean-Marc Moschetta, *Shock wave instability and the carbuncle phenomenon: Same intrinsic origin?*, *Journal of Fluid Mechanics* **417** (2000), 237–263.

- [46] Alexander V. Rodionov, *Artificial viscosity in Godunov-type schemes to cure the carbuncle phenomenon*, Journal of Computational Physics **345** (2017), 308–329.
- [47] Alexander V. Rodionov, *Artificial viscosity to cure the carbuncle phenomenon: The three-dimensional case*, JCoPh **361** (2018), 50–55.
- [48] Alexander V. Rodionov, *Artificial viscosity to cure the shock instability in high-order Godunov-type schemes*, Computers & Fluids **190** (2019), 77–97.
- [49] P. Roe, H. Nishikawa, F. Ismail, and L. Scalabrin, *On carbuncles and other excrescences*, AIAA paper (2005), no. 4872.
- [50] Philip L. Roe, *Approximate Riemann solvers, parameter vectors, and difference schemes*, J. Comput. Phys. **43** (1981), no. 2, 357–372.
- [51] Richard Sanders, Eric Morano, and Marie-Claude Druguet, *Multidimensional dissipation for upwind schemes: Stability and applications to gas dynamics*, Journal of Computational Physics **145** (1998), no. 2, 511–537.
- [52] Zhijun Shen, Wei Yan, and Guangwei Yuan, *A robust HLLC-type Riemann solver for strong shock*, Journal of Computational Physics **309** (2016), 185–206.
- [53] Shu sheng Chen, Chao Yan, and Xing hao Xiang, *Effective low-Mach number improvement for upwind schemes*, Computers & Mathematics with Applications **75** (2018), no. 10, 3737–3755.
- [54] Shu sheng Chen, Chao Yan, Bo xi Lin, Li yuan Liu, and Jian Yu, *Affordable shock-stable item for Godunov-type schemes against carbuncle phenomenon*, Journal of Computational Physics **373** (2018), 662–672.
- [55] Chi-Wang Shu and Stanley Osher, *Efficient implementation of essentially non-oscillatory shock-capturing schemes*, J. Comput. Phys. **77** (1989), no. 2, 439–471.
- [56] Sangeeth Simon and J.C. Mandal, *A cure for numerical shock instability in HLLC Riemann solver using antidiffusion control*, Computers & Fluids **174** (2018), 144–166.
- [57] Eleuterio F. Toro, *Riemann solvers and numerical methods for fluid dynamics. A practical introduction. 3rd ed.*, Berlin: Springer, 2009 (English).
- [58] Guohua Tu, Xiaohui Zhao, Meiliang Mao, Jianqiang Chen, Xiaogang Deng, and Huayong Liu, *Evaluation of Euler fluxes by a high-order CFD scheme: shock instability*, International Journal of Computational Fluid Dynamics **28** (2014), no. 5, 171–186.
- [59] Paul Woodward and Phillip Colella, *The numerical simulation of two-dimensional fluid flow with strong shocks.*, J. Comput. Phys. **54** (1984), 115–173.

- [60] Wenjia Xie, Wei Li, Hua Li, Zhengyu Tian, and Sha Pan, *On numerical instabilities of Godunov-type schemes for strong shocks*, *Journal of Computational Physics* **350** (2017), 607–637.
- [61] Wenjia Xie, Ran Zhang, Jianqi Lai, and Hua Li, *An accurate and robust HLLC-type Riemann solver for the compressible Euler system at various Mach numbers*, *International Journal for Numerical Methods in Fluids* **89** (2019), no. 10, 430–463.
- [62] D. W. Zaide and P. L. Roe, *Flux functions for reducing numerical shockwave anomalies*, *sign* **1** (2012), 2.
- [63] Daniel W. Zaide and Philip L. Roe, *Shock capturing anomalies and the jump conditions in one dimension*, 20th AIAA CFD Conference, 2011.
- [64] Daniel Wei-Ming Zaide, *Numerical shockwave anomalies*, Ph.D. thesis, The University of Michigan, 2012.
- [65] Shuhai Zhang, Hanxin Zhang, and Chi-Wang Shu, *Topological structure of shock induced vortex breakdown*, *Journal of Fluid Mechanics* **639** (2009), 343–372.